Hybrid structure based high performance SPR sensor: a numerical approach of structure optimization for DNA hybridization

Md. Biplob Hossain[1] · Md. Alamgir Kabir[2] · Md. Mizanur Rahman[3] ·
Sourav Roy[4] · Lway Faisal Abdulrazak[5,6] · Md. Sanwar Hossain[2] · Nibir Mondol[7] ·
Mohammed Hadifur Rahman[8] · Khondoker Ziaul Islam[2] · M Ilius Pathan[3]

Abstract
A MoS$_2$-Graphene hybrid layer Based High Performance Refractive Index SPR Sensor is illustrated in this paper. Intended for the enhancement of sensor angular sensitivity (S), signal to noise ratio (SNR), quality factor (QF), first of all, the impact of gold layer thickness is investigated and optimized to 40 nm, after then the MoS$_2$ and graphene coting layers are optimized to four (4) and three (3) layers, respectively. Further that, at this optimum structure, the minimum reflectance and SPR angle are decorated. It is seen that the angular sensitivity of the optimum assembly, improved to excellent value of 130 deg-RIU^{-1} with improved angular SNR of 1.37 and QF of 17.02 RIU^{-1}. At the end of this paper, an analysis specifically for numerically DNA hybridization is considered.

Keywords SPR · SNR · Sensitivity · QF

1 Introduction

Surface plasmon resonance (SPR) founded optical sensing technology has assumed a pivotal part in monitoring diverse biochemical interactions in particular binding of proteins (Hossain et al. 2020a; Isti et al. 2020; Goyal and Saini 2020), haemoglobin concentration (Goyal and Pal 2020) as well as DNA-DNA hybridization (Ebrahimi et al. 2018). SPR, an optical exhibition, gives a label-free mechanism of investigating binding interactions between a biomolecule and an analyte (Saha et al. 2020, 2019a; Nico and Fischer 2010; Liedberg et al. 1983). The SPR has a developing enthusiasm for the application of optics and optoelectronics. Other than that, SPR is broadly employed as plasmonic devices (Hossain et al. 2019a), biomedical sensing (Saha et al. 2019b; Bashiri et al. 2019), optical solar cell (Akimov and Koh 2010), organic light emitting diode (OLED) (Kretschmann and Raether 1968), and so on.

✉ Md. Biplob Hossain
  biplobh.eee10@gmail.com

Extended author information available on the last page of the article

The propagation of the SPs especially relies proceeding the effective RI of the sensing medium contiguous the metal that creates it an incredible technique to capture the modifications in RI of a sample by reason of binding actions and in this way becomes useful for bio-sensing application (Filion-Côté et al. 2014). Surface plasmon wave (SPW) can get energized when the incident optical signal gratifies a definite incident state (Hossain et al. 2019b), and the excitation for Surface Plasmons (SPs) are fundamentally guided by the part of the fierce reflectance dip (Lin et al. 2016). Biosensors using SPs scheme possess speedy and extremely responsive to biomolecular sensing (Hossain et al. 2019c; Sreekanth et al. 2013) which able it more convenient than fluorescence-based optical sensors that require more time and has high molecular binding disorder (Jacob 2012).

The attenuated total reflection (ATR) designed SPR biosensor renders in two activity mode: First mood by angular inquisition where the wavelength of incident light signal is fixed, and the input angle is changed or second one by wavelength inquisition where the entering angle is fixed and the wavelength is varied (Pockrand et al. 1978). The performance of SPR sensor enhances largely at the point when MoS_2 and graphene are utilized in place of detecting improvement layer (Pockrand 1978; Wolfbeis and Weidgans 2006; Rahman et al. 2017a; Soheilifar and Zarrabi 2019; Verma et al. 2015; Heydari et al. 2017). The SPR sensors are frequently utilized in the field of enzyme detection (Wolfbeis and Weidgans 2006), protein-DNA (Wolfbeis and Weidgans 2006), food safety (Pumera 2011), communication channel security enhancement (Sarker et al. 2020; Islam et al. 2020; Avazov et al. 2017), biological and biochemical sensing applications(Maurya et al. 2015b) for example, film characterization (Mollah et al. 2020), and beam polarization selection (Lee et al. 2015), DNA-DNA hybridization (Lee et al. 2015), protein–protein (Kim et al. 2006; Madeira et al. 2011), enzyme–substrate or inhibitor (Yuan et al. 2011), wireless & remote sensing (Shahzad et al. 2019; Hossain et al. 2018) and so forth. The MoS_2 and Graphene, both are 2D material of mono atomic thickness. They both have numerous properties to be specific low reluctance, high carrier mobility, high optical transparency, tenability and so on (Sakib et al. 2020; Hossain et al. 2016, 2015; Rana et al. 2015; Hossain and Rana 2015a). For the excitation and spread of surface plasmons, their utilization have been verified experimentally and theoretically (Hossain et al. 2020b).

In this paper, A SPR sensor along with optimized structure of MoS_2/graphene is utilized for the application of DNA hybridization. The MoS_2/graphene is profoundly responsive to the charged analytes for example, ions, DNAs, body cells, and so on. It turns into a perfect material for high performance sensors due to having an electric field around graphene. Because of the adsorption of DNA on MoS_2 as well as graphene, it was demonstrated experimentally that charge can be moved through DNA bio focuses to MoS_2/graphene surface. The DNA bases and the carbon atoms bonds is a kind of Van der Waals bolding (π stacking) (Shushama et al. 2017a). Because of this, MoS_2/graphene has abrupt change in refractive index close the $_{MoS2}$/graphene-sensing layer interface. For the increment of sensor angular sensitivity (S), signal to noise ratio (SNR), quality factor (QF), most importantly, the impact of including MoS_2/graphene layer is investigated and afterward the number of their layers are optimized to four and three layers. Subsequently, at these ideal layers, the SPR curves are plotted and correlation of sensor sensitivity, signal to noise ratio, quality factor is made among the current works. It is seen that the angular sensitivity of the upgraded MoS_2/graphene layers-based sensor is enhanced to a standard value of 130 deg-RIU^{-1} having improved angular SNR of 1.37 and QF of 17.02 RIU^{-1}. The article is systematized as given. In Sect. 2, the Computational Design Methodology of the proposed work is described which is covered by two subsections, one is Organizational Design and another is Mathematical Design. In section III, the Numerical results and

discussion are described under a number of tables, equations and figures. First portion of the numerical results and discussion section is exemplified Structure Optimization on Sensor Performance Analysis and the rest exemplified the DNA detection approach.

2 Computational design methodology

2.1 Organizational design of proposed sensor

The offered SPR design is composed by five layers, the design of that is appeared in Fig. 1. The entering optical signal along the transverse magnetic (TM) polarization is one of the furthermost significant conditions for the stimulation of SPs (Soheilifar and Zarrabi 2019). The 633 nm is chosen as operating wavelength because the optical nonlinearity can be upgraded at low wavelength (O'Brien et al. 2014). All through the photon energy range, micro band optical transitions happen because MoS_2/graphene has band structure (Luo et al. 2016; Maurya et al. 2015a). Subsequently, the whole performance of the biosensor is heightened along with negligible Kerr effect at 633 nm wavelength (Rahman et al. 2017b). For angular interrogation, we utilized Fresnel multilayered system to model the offered sensor that is described in detail in literature (Rahman et al. 2017a, 2017b, 2016; Shushama et al. 2017a, 2017b; Hossain and Rana 2016, 2015b). In the direction of giving additional momentum along the entrance light, high propagation constant supported photonic crystals should be utilized (Isti et al. 2020), to satisfy this condition, we indicated high RI based prism, for example, SF11 optical prism as a foundation layer of high RI (n_p) of 1.7786 (Rahman et al. 2017b). As a second layer, we utilized gold (RI, $n_{Au} = 0.1838 + i$ 3.4313 of optimized thickness (d_{Au}), to keep up both improve angular QF and SNR. At the point when the propagation constant of entering light remains confined at the interface and decays exponentially in the transverse directions, resonant excitation of photon-electron coupling happens (Shushama et al. 2017a, 2017b).

The momentary tail of SPR is highly responsive to the modification in complex RI of metalic coating, neighboring dielectric analyte and their configural sizes (Soheilifar and Zarrabi 2019; Shushama et al. 2017a), that resulted extreme sensor angular sensitivity (Soheilifar and Zarrabi 2019). For quickening responsive change of tail in SPR

Fig. 1 Schematic of 5-layered proposed design: prism/gold/MoS2/Graphene/sensing medium
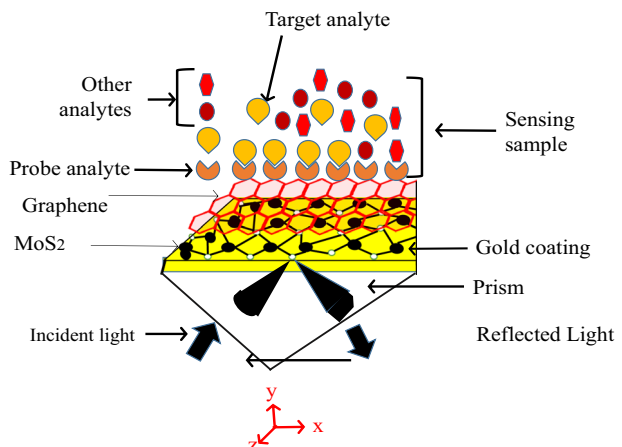
momentary wave to acquire extreme sensor angular sensitivity with standard detection accuracy (DA), we selected MoS_2 and graphene as 3rd and 4th layer which has high complex RI (RI, $n_G = 3.0 + i\ 1.1487$ and $n_M\ 5.9 + i\ 0.8$ (Shushama et al. 2017b; Rahman et al. 2016)) alo*ng* with high carrier mobility, high optical transparency, exceptional mechanical flexibility, mechanical strength (Hossain et al. 2016, 2015; Rana et al. 2015; Hossain and Rana 2015a), low resistivity, tunable conductivity, and extreme mode confinement (Hossain et al. 2016). Also, last layer is water(RI $n_5 = 1.33$) as bare sensing medium that manages better absorption of DNA molecules (Ball and Ramsden 1998; Diéguez et al. 2009).

3 Mathematical design of proposed sensor

The incident light is formed a momentary signal at the moment of passing through SF11 prism and it is finally reflected from the SF11 prism-Au interface. For Transvers Magnetic-polarized optical signal, the reflectance is exposed as (Rahman et al. 2017a; Shushama et al. 2017a):

$$\text{Ro} = |r_o|^2 \tag{1}$$

where

$$r_o = \frac{(B_{11} + B_{12}n_N)n_1 - (B_{21} + B_{22}n_N)}{(B_{11} + B_{12}n_N)n_1 + (B_{21} + B_{22}n_N)} \tag{2}$$

In Eq. (5), F is well-defined in (Shushama et al. 2017a) as:

$$B_{ij} = \left[\prod_{k=2}^{4-1} \left(\begin{array}{cc} \cos\beta_k & -\frac{i\sin\beta_k}{n_k} \\ -in_k\sin\beta_k & \cos\beta_k \end{array} \right) \right]_{ij} = \left[\begin{array}{cc} B_{11} & B_{12} \\ B_{21} & B_{22} \end{array} \right] \tag{3}$$

Here n_k is arbitrary transverse refractive indices of the comparing k^{th} layer which can be illustrated by the relation (Rahman et al. 2017a)

$$n_k = \left[\frac{\mu_k}{\varepsilon_k} \right]^{1/2} \cos\theta_k = \sqrt{\frac{\varepsilon_k - (n_p\sin\theta_{in})^2}{\varepsilon_k^2}} \tag{4}$$

And β_k is arbitrary phase constant of the corresponding k^{th} layer which can be explained by the relation (Rahman et al. 2017a):

$$\beta_k = \frac{2\pi}{\lambda}n_k\cos\theta_k(z_k - z_{k-1}) = \frac{2\pi}{\lambda}d_k\sqrt{\varepsilon_k - (n_p\sin\theta_{in})^2} \tag{5}$$

Here, z_k is the wave impedance of kth layer and is characterized as (Hossain and Rana 2016):

$$z_k = \frac{k_{light}n_k\cos\theta_k}{(2\pi c/\lambda_{633})\varepsilon_k^2} \tag{6}$$

And θ_k is the incident angle of kth layer, is expressed as (Hossain and Rana 2016):

$$\theta_k = a\cos\left(\sqrt{1 - (n_{k-1}/n_k)\sin^2\theta_{in}}\right) \tag{7}$$

In Eq. (1) to (7), n_1 is the refractive index of prism, θ_{in} is the 1st layer entrance angle demonstrated in Eq. (1), ϵ_k is the permittivity of a specific kth layer, d_k is the thickness of specific kth layer (thickness of graphene $d_G = G \times 0.34$ nm, thickness of MoS_2 $d_M = M \times 0.65$ nm, here G and M are the graphene and MoS_2 layers, respectively, thickness of gold d_{Au} is needed to be optimized) individually.

The RI of the detecting layer varies by reason of deluging probe DNA (pDNA) to the detecting layer. The effective RI of detecting layer after absorption of DNAs molecules is precisely represented as (Rahman et al. 2017a, 2017b; Shushama et al. 2017a, 2017b):

$$n^1_{sens} = n^0_{sens} + c_a \frac{\Delta n}{\Delta c} \tag{8}$$

Here, n^1_{sens} is the effective refractive index of the detecting layer after absorption of DNAs solutions, n^0_{sens} is the effective refractive index of the detecting layer before absorption of DNAs solutions, c_a is the concentration of absorbed DNAs, and $\Delta n/\Delta c$ is the RI progress because of the adsorbate DNA molecules. The effective refractive index development parameter ($\Delta n/\Delta c$) is a value of 0.18 ± 0.03 cm³/gm, while using water (Sreekanth et al. 2013). At resonance point, the wave vector of entering wave identical to SPW. Variation of the concentration (density) of detecting layer because of the immobilization of DNAs pursuits the variation of local RI (n_S) of that sensing medium narrated by Eq. (8). At a constant wavelength the SPR condition is attained when the incident angle is varied in which reflectance intensity (R) of the reflected wave is lowest and its spectra (normalized reflected power) show dip. The performance of SPR sensor is fundamentally analyzed based on its angular sensitivity (S), detection accuracy (DA), and the quality factor (QF) which are elaborately described in literature (Hossain et al. 2019b, 2019c).

4 Numerical results and discussions

4.1 Structure optimization and sensor performance parameters analysis

In the beginning, a SPR curve of simple structure having monolayer (G & M = 1) of graphene and MoS_2 with sensing layer effective RI (ERI) of 1.33, as shown in Fig. 2, has been considered everywhere to observe the outcome due to the variation of gold layer thickness on sensor performance. And from this outcome, the thickness of gold layer can be optimized to ensure superior sensor performance. The changing characteristics of gold layer thickness has played a weighty impact on reflectance and SPR angle. The Fig. 2 represents the modification of minimum reflection versus SPR angle characteristics with increment of Au thickness from 20 to 60 nm. It is evident from Fig. 2; due to increase or decrease of thickness from 40 nm, SPs become damped. So that, the minimum reflected intensity in reflectance curve is observed at 40 nm thickness of gold layer which shows the strong coupling of incident light to SPs and results in efficient excitation of SPs (Rahman et al. 2016, 2018). As a result of increasing or decreasing of thickness from 40 nm, full width half maximum (FWHM) increases (Shushama et al. 2017a, 2017b; Farajollahi et al. 2015). It has been observed from the definition of SNR and QF that with the increase in FWHM linearly decreasing angular SNR and angular QF which also evidenced from Table 1.
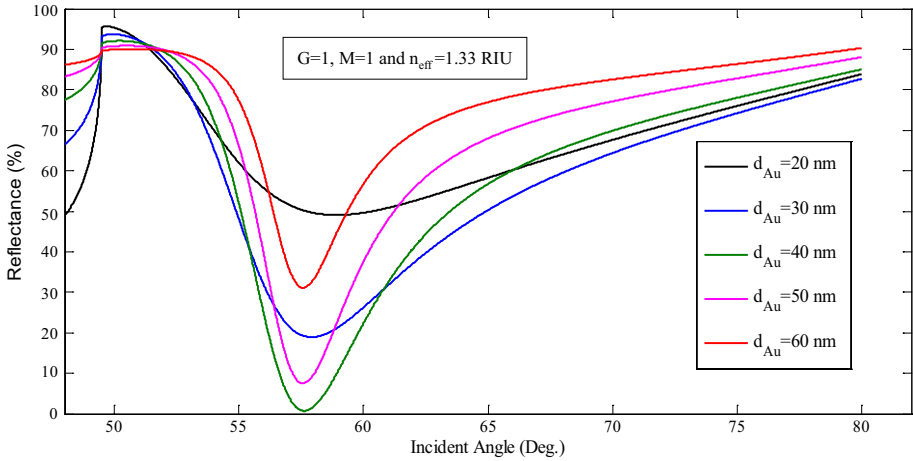
Fig. 2 Variation of minimum reflectance vs incident angle characteristics curve for various thicknesses of gold

Table 1 Sensitivity (S), Signal to Noise Ratio (SNR) and quality factor (Q.F) for various thickness of Au layers

d_{Au} (nm)	n_{eff} = 1.33 RIU		n_{eff} = 1.41 RIU		$\Delta\theta_{SPR}(Deg.)$	$\Delta\theta_{0.5}(Deg.)$	S (Deg./RIU)	SNR	QF RIU^{-1}
	R_{min}	θ_{SPR}(Deg.)	R_{min}	θ_{SPR}(Deg.)					
20	0.3782	45.0000	0.3582	46.0000	1.00	16.00	12.50	0.78	9.75
30	0.1893	57.9400	0.1864	63.9400	6.00	11.80	75.00	6.35	79.37
40	0.0072	57.5600	0.0040	64.2800	6.72	10.10	84.00	8.31	103.87
50	0.0753	57.5200	0.0937	64.2500	6.69	10.50	83.62	7.96	99.50
60	0.1613	57.5800	0.3436	64.2300	6.65	11.30	83.12	7.35	91.87

Figure 2 has been considered to describe the effect of sensor performance parameters (sensor angular sensitivity, angular SNR, angular QF) on the change of gold layer thickness. Here, the modification of minimum reflectance, SPR angle and FWHM have been calculated for n_{eff} = 1.33 RIU (bare sensor, NO DNAs) and n_{eff} = 1.41 RIU (sensing layer contains 1000 nM concentrated target DNAs) and fixed wavelength of 633 nm. The obtained outcomes are described in Table 1 for gold layer thickness of d_{Au} = 20 nm, 30 nm, 40 nm, 50 nm and 60 nm, respectively. When the ERI increases from 1.33 RIU to 1.41 RIU (Δn_{eff} = 0.08 RIU), 2nd row in Table 1 shows that the SPR angle increases from 45.00 to 46.00 degree (change in SPR angle; $\Delta\theta_{SPR}$ = 1.00 Deg., and change in spectral width; $\Delta\theta_{0.5}$ = 12.50 Deg.) at d_{Au} = 20 nm, 3rd row in Table 1 shows that the SPR angle shifts from 57.94 to 63.94 degree (change in SPR angle; $\Delta\theta_{SPR}$ = 6.00 Deg., and change in spectral width;$\Delta\theta_{0.5}$ = 11.80 Deg.) at d_{Au} = 30 nm, 4th row in Table 1 shows that the SPR angle shifts from 57.56 to 64.28 degree (change in SPR angle;$\Delta\theta_{SPR}$ = 6.72 Deg., and change in spectral width;$\Delta\theta_{0.5}$ = 10.10 Deg.) at d_{Au} = 40 nm, 5th row in Table 1 shows that the SPR angle shifts from 57.52 to 64.25 degree (change in SPR angle;$\Delta\theta_{SPR}$ = 6.69 Deg., and change in spectral width;$\Delta\theta_{0.5}$ = 10.50 Deg.) at d_{Au} = 50 nm and 6th row in Table 1

shows that the SPR angle shifts from 57.5800 to 64.2300 degree (change in SPR angle; $\Delta\theta_{SPR} = 6.65$ Deg., and change in spectral width; $\Delta\theta_{0.5} = 11.30$ Deg.) at $d_{Au} = 60$ nm, respectively. The modification of minimum reflectance, SPR angle and spectral width have been summarized in Table 1 for different gold layer thickness with monolayer of graphene and MoS_2.

It is professed from Table 1 that the maximum angular sensitivity, angular SNR and angular QF and lowest changed minimum refractive index have been attainable at 40 nm. A perfect sensor must have a sensitivity, angular SNR, QF as high as possible with lowest minimum reflectance. However, to maintain high sensitivity along with both SNR and QF, we have well thought-out of 40 nm all over the study.

Secondly in this section, the optimization of the number of MoS_2 and graphene are analyzed by keeping optimized thickness of gold layer equals to 40 nm. Firstly, the impact of addition of graphene on angular sensitivity, angular SNR and angular QF has been numerically discussed. The number of graphene layers have momentous influences in the enhanced performance and upgrading of angular sensitivity for the raised SPR sensor. Hence, we look into the fluctuation of refractive index for different graphene layers in Fig. 6 where MoS_2 layers kept constant to one (M = 1) to ensure how much graphene layer can alone play impact on sensor performance. The number of carrier changes with the introduction of electron-rich DNA molecules in the graphene layer, which leads to the variation of the wave vector (Shushama et al. 2017a), finally a variation in SPR angle is happened.

Here in Fig. 3, we determine how SPR angle shifts with the addition of graphene layers, we have enumerated SPR curves for several layers of graphene at a constant wavelength of 633 nm after the addition of 1000 nM target-DNAs molecules (sensor, present both water and target DNAs). The results are in Fig. 3(a) and (b). The momentous right move of SPR angle is a symbol of acknowledgment proper orientation of tangible mutated sequence interaction with probe DNAs, as well as that clarifies the sensing of DNA-DNA hybridization (Shushama et al. 2017a, 2017b; O'Brien et al. 2014; Luo et al. 2016; Maurya et al. 2015a; Rahman et al. 2017b; Hossain and Rana 2016, 2015b). We determine the angular sensitivity (S), angular SNR and angular Q.F; these outcomes are presented in Table 2, which focuses the difference on performance parameters. It is observed from Table 2, It is possible to enrich the angular sensitivity by including graphene layers. For these configurations, we determined $\Delta n_S = 0.08$ by incorporating Eq. (8) when 1000 nM complementary target DNA is present in the sensor.

Also, it is realized from Table 2 that the SPR angle moves toward more excellent value on the growth of the number of graphene layers (Hossain and Rana 2015b). This moving of resonance angle toward more prominent value alongside the expanded width of the reflectance curve looks like the rampant variance in the SPR signal initiated by graphene coating onto metal film (Hossain and Rana 2016; Shushama et al. 2017b). This extraordinary variance in the SPR curve at long last outcomes in the up-gradation of sensitivity (Rahman et al. 2017a). This exalt sensitivity happens as a result of the moving of θ_{SPR}, that is because of the absorption ability of biomolecules (Hossain et al. 2015), high fluorescence quenching ability of graphene (Rana et al. 2015). Furthermore, Table 2 represents the evaluated outcomes for angular SNR and QF for graphene based offered SPR sensor. It is sure from Table 2 that angular SNR and QF are reducing slowly because of the increasing graphene layer of the biosensors.

Now, we evaluate the optimization of graphene layers which secures high angular sensitivity along with enhance angular SNR and QF of the offered SPR optical sensor by change the layers of graphene from 1 to 10. As shown in Fig. 4, the elevated sensitivity & SNR
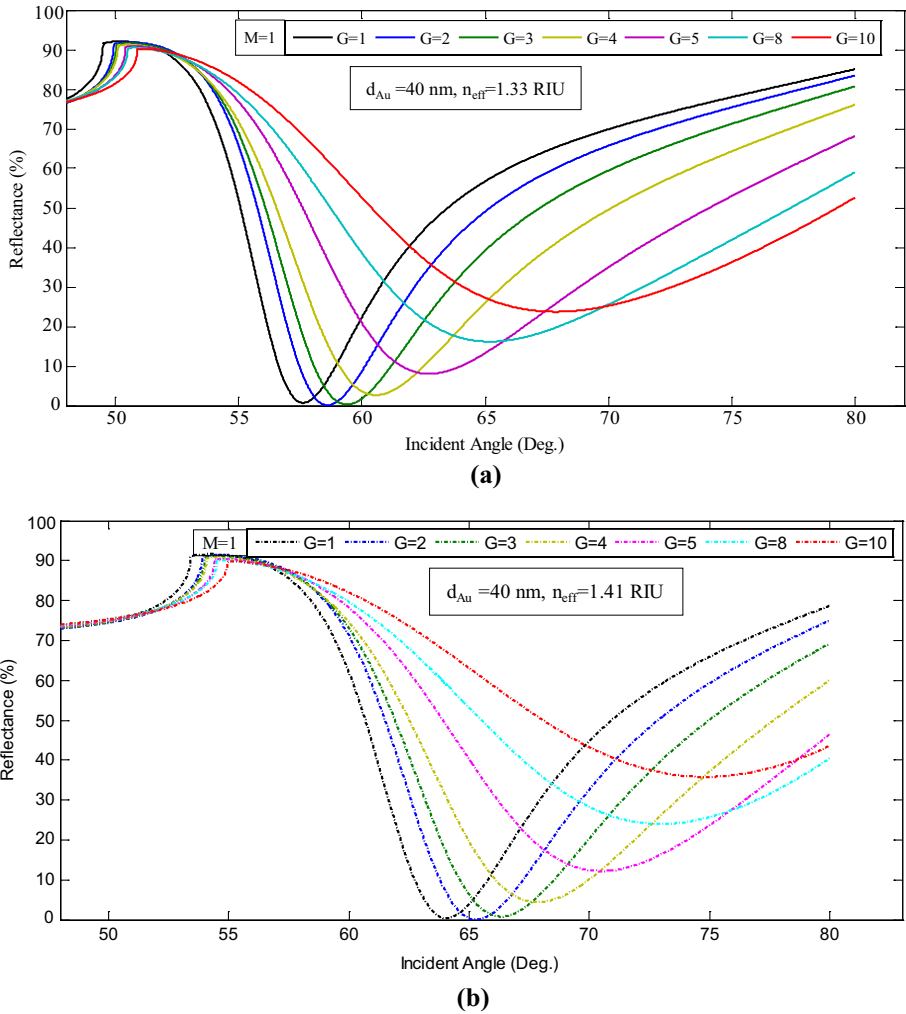
Fig. 3 SPR curve for different graphene layers **a** before absorption of DNAs, **b** After absorption of 1000 nM complementary target DNAs (ctDNAs)

as well as sensitivity & QF can be attained at the time when the number of the graphene layer is in between 4 and 5. Therefore, we choose the optimum graphene layer as 4 in the proposed SPR biosensor to ensure also fabrication simplicity. Nevertheless, they are yet acceptable for the sensing of DNA-DNA hybridization.

In analogous way, the impact of adding MoS_2 on the performance parameters are analyzed and optimized in terms of angular SNR, sensitivity (S), and angular QF. These results are also shown in Fig. 5 and tabulated in Table 3. Hence from the close observation of Fig. 6, the maximum angular sensitivity with angular SNR as well as angular QF with angular SNR can be attained at the time when the number of the MoS_2 layer is 3. Therefore, we choose the optimum MoS_2 layer as 3 in the proposed SPR biosensor. Now, the performance parameters are analyzed and measured in terms of angular SNR, sensitivity (S), and angular QF for our optimized structure (tetra layers of graphene and try layers of

Table 2 Sensitivity (S), SNR and QF for various graphene layers

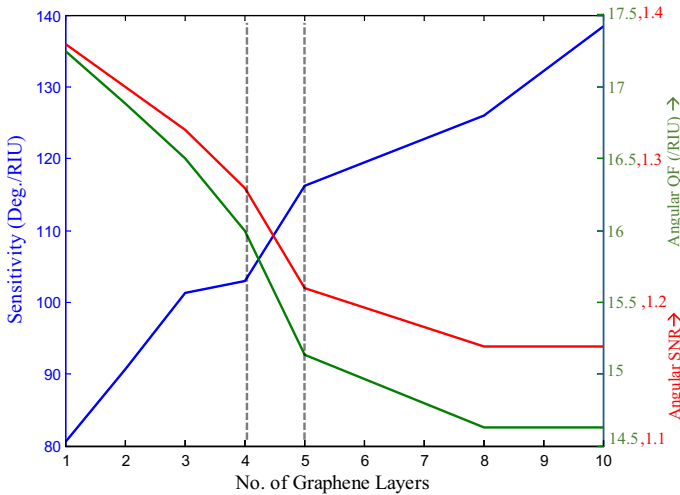| No. of graphene layer (G)	$\theta_{SPR}^{n=1.33}$(Deg.)	$\theta_{SPR}^{n=1.41}$(Deg.)	$\theta_{0.5}^{n=1.33}$(Deg.)	$\theta_{0.5}^{n=1.41}$(Deg.)	Change of SPR angle $(\Delta\theta_{SPR} = \theta_{SPR}^{1.41} - \theta_{SPR}^{1.33})$	Change of spectral width $(\Delta\theta_{0.5} = \theta_{0.5}^{1.41} - \theta_{0.5}^{1.33})$	Sensitivity (S) Deg./RIU	SNR	QF (RIU^{-1})
1	57.56	64.00	55.84	60.56	6.44	4.72	80.50	1.37	17.10
2	58.36	65.62	55.50	60.88	7.26	5.38	90.75	1.35	16.88
3	59.02	67.12	55.74	61.92	8.10	6.18	101.25	1.32	16.50
4	60.30	68.54	55.92	62.40	8.24	6.48	103.00	1.28	16.00
5	62.50	71.80	57.15	64.85	9.30	7.70	116.25	1.21	15.13
8	64.00	74.08	58.00	66.62	10.08	8.62	126.00	1.17	14.63
10	65.85	76.92	59.06	68.55	11.07	9.49	138.38	1.17	14.63

Fig. 4 Variation of angular sensitivity (blue color), angular SNR (red color) and angular QF(green color) as the function of graphene layers (solid line). (Color figure online)

MoS$_2$). We calculated for tetra layers of graphene and try layers of MoS$_2$ that SPR angle and spectral width point 67.13 Deg. and 59.54 Deg., respectively, for bare sensor (black line) and 77.53 Deg. and 67.18 Deg., respectively after adsorption of 1000 nM target DNAs molecules at operating wavelength of 633 nm. By using G = 4 and M = 3, we have obtained the alteration of SPR angle and the change of spectral width 10.40 degree and 7.64 Deg., respectively. For this optimization configuration, the calculated angular sensitivity, SNR and QF are 130 Deg./RIU, 1.37 and 17.02 RIU^{-1}. This improved performance happens by reason of the changing of θ_{SPR}, which is attributable to the adsorption capability of graphene (Filion-Côté et al. 2014) and high fluorescence quenching capability of MoS$_2$ (Hossain et al. 2019c). It is obvious from this study that SNR and QF are lessening slowly owing to the increase of biosensor layers. Though, the angular SNR and QF are reduced as a consequence of their kith and kin to spectral width, nevertheless they are satisfactory for the sensing of DNA-DNA hybridization in where angular sensitivity is the important issue.

5 DNA hybridization detection approach

In this subsection, the DNA Hybridization Detection Approach has been described in detail, the component, where pDNAs is detected by the offered MoS$_2$/graphene-based SPR sensor, is appeared in Fig. 1. In Fig. 7, an optical system consisting five-layers and individual SPR curves previously (blue line) and after (red line) accessment of probe DNA (pDNA) are appeared. The outcome shows that the SPR angle is 67.13 degree in the case of bare sensor and 71.19 degree after addition of pDNAs.

On account of the modification of the concentration of detecting layer, the effective refractive index (ERI) is additionally varied as per Eq. (8). Since the effective refractive index (ERI) transforms, it needs adjustment in SPR condition. The SPR angle is right shifted by 4.04 degree due to the addition of 1000 nM pDNAs shown in Fig. 7. This
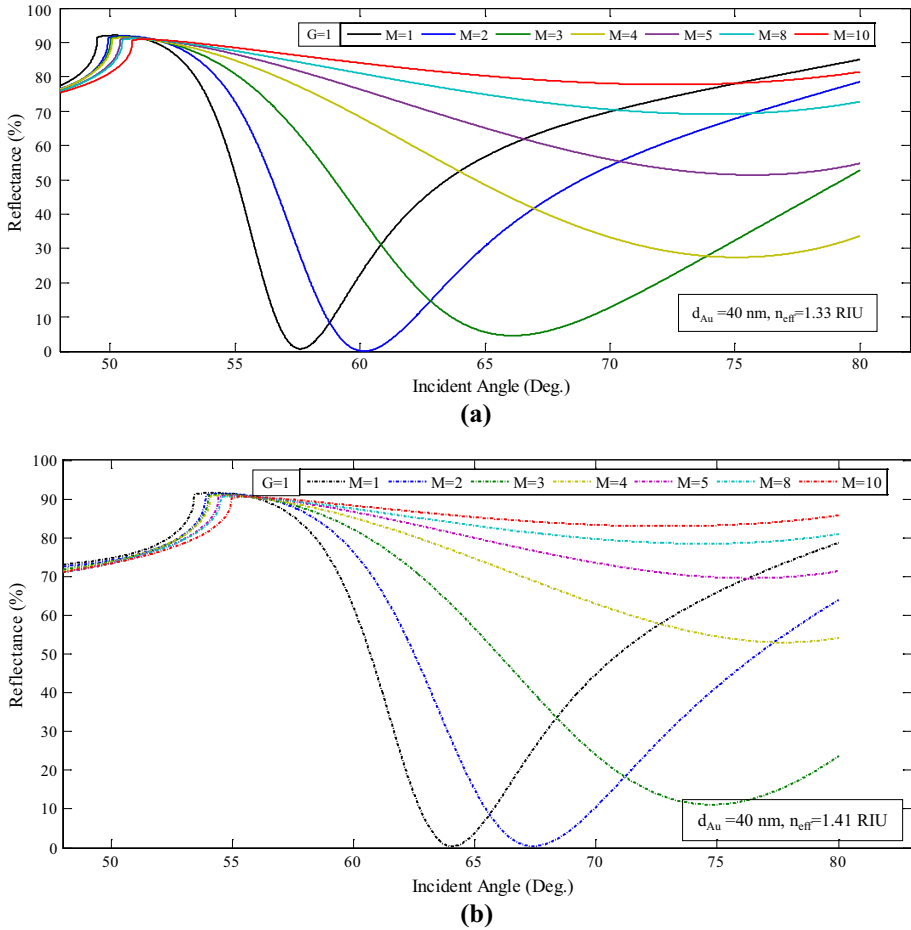
Fig. 5 SPR curve for different MoS$_2$ layers-based sensor **a** before absorption of DNAs, **b** after absorption of 1000 nM complementary target DNAs (ctDNAs) of 633 nm operating wavelength

outcome surely be acknowledged by the dependence of SPR angle on pDNAs and hybridization of the ctDNAs (Saha et al. 2019a).

During the occasion when two single-stranded complementary target DNAs (ctDNAs) (one is probe and other is complementary target) are bonded together and made a dual-stranded DNAs helix structure, this is perceived as per a complementary hybridization event (Ebrahimi et al. 2018). The offered design clarifies the conduct to investigate the complementary hybridization between pDNAs and ctDNAs which are pre immobilized on MoS$_2$/graphene surface. In addition, the proposed SPR device can likewise ready to separate between complementary and single-base-mismatched DNA molecules, which is significant for the characterization of changes and single-mismatched hybridization event.

The circumstance when diverse concentrated ctDNAs are included to 1000 nM pDNAs has been appeared in Fig. 8 and individual color line demonstrates diverse concentrated ctDNAs molecules. According to the attained data, the SPR angle and minimum reflectance have played a significant role to detect hybridization. These parameters will change

Table 3 Sensitivity (S), SNR and QF for various MoS_2 layers

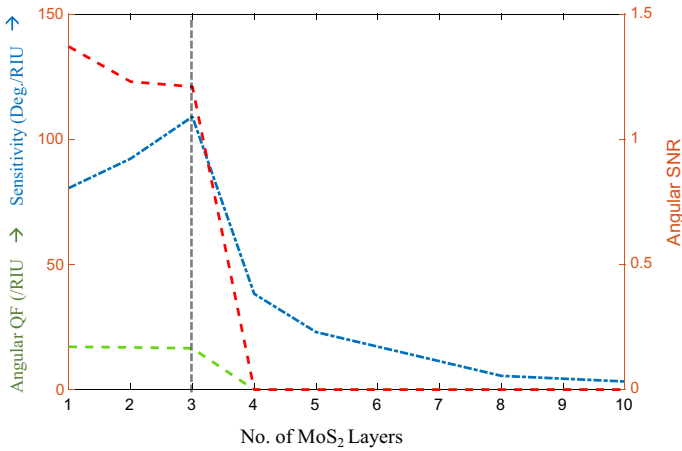| No. of MoS_2 layer (M)	$\theta_{SPR}^{n=1.33}$	$\theta_{SPR}^{n=1.41}$	$\theta_{0.5}^{n=1.33}$	$\theta_{0.5}^{n=1.41}$	Change of SPR angle ($\Delta\theta_{SPR} = \theta_{SPR}^{1.41} - \theta_{SPR}^{1.33}$)	Change of spectral width ($\Delta\theta_{0.5} = \theta_{0.5}^{1.41} - \theta_{0.5}^{1.33}$)	Sensitivity (S) Deg./RIU	SNR	QF (RIU^{-1})
1	57.56	64.00	55.84	60.56	6.44	4.72	80.5	1.37	17.10
2	60.12	67.50	56.50	62.50	7.38	6.00	92.25	1.23	16.88
3	66.28	75.00	58.92	66.14	8.72	7.22	109.00	1.21	16.50
4	74.44	77.50	64.56	~Inf	3.06	~Inf	38.25	~0	~0
5	76.26	78.10	75.88	~Inf	1.84	~Inf	23.00	~0	~0
8	75.68	76.12	~Inf	~Inf	0.44	~Inf	5.50	~0	~0
10	74.82	75.08	~Inf	~Inf	0.26	~Inf	3.25	~0	~0

Fig. 6 Variation of angular sensitivity (blue color), angular SNR (red color) and angular QF(green color) as the function of MoS$_2$ layers (dashed line)

Fig. 7 SPR response curve for the offered design: the SPR angle is 67.13 Deg. in the case of bare sensor and 71.19 Deg. after the addition of 1000 nM pDNAs
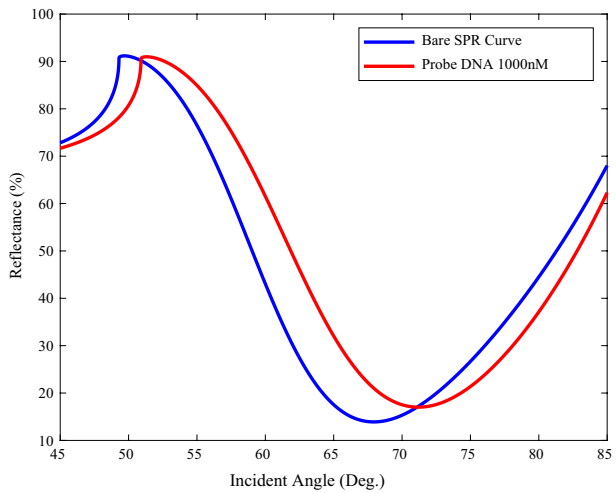
when ctDNAs are joined to pDNAs. Judgment will be decided dependent on the alteration of SPR angle and minimum reflectance. The SPR angle and minimum reflectance are determined to 0.3028 & 77.53 degree for 1000 nM concentrated ctDNAs, 0.3203 & 77.87 degree for 1001 nM concentrated ctDNAs, 0. 3584 & 78.47 degree for 1010 nM concentrated ctDNAs, and 0. 4222 & 79.18 degree for 1100 nM concentrated ctDNAs, respectively. The numerical information depicts strong reliance of the SPR angle on the concentration increase. The moving of the SPR angle happens due to the ctDNA molecules are responded with both of MoS$_2$ and graphene surface and produced n-doping effect. The noteworthy increment of the SPR angle is an indication of probe-target matching in DNAs hybridization. In the study of detection approach, at first, the values of $\left(\Delta R_{min}^{ctDNA-pDNA} \right)_{min}$ and $\left(\Delta \theta_{SPR}^{ctDNA-pDNA} \right)_{min}$ have been calculated by using the Eq. set (9). And defining these values as threshold parameters.

Fig. 8 SPR response curve for the offered design: the SPR angle is 71.19 Deg. after the addition of 1000 nM pDNAs and 77.53 degree after the addition of 1000 nM ctDNA
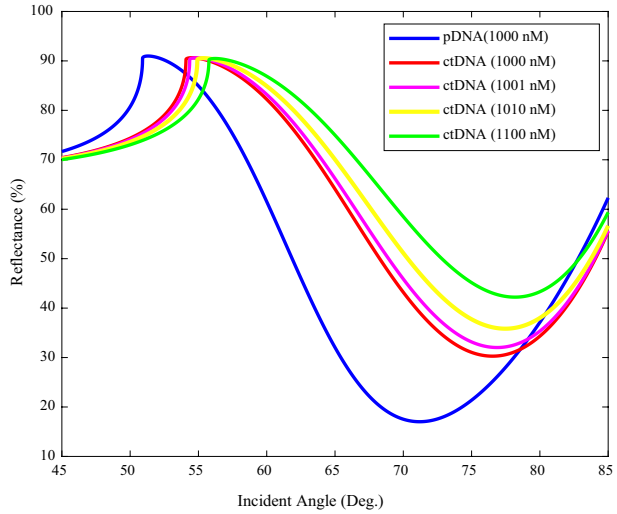
$$(\Delta R_{min}^{(ctDNA-pDNA)})_{min} = R_{min}^{(ctDNA=1000nM)} - R_{min}^{(pDNA=1000nM)} = 0.3028 - 0.1702 = 0.1326 \tag{9a}$$

$$(\Delta\theta_{SPR}^{(ctDNA-pDNA)})_{min} = \theta_{SPR}^{(ctDNA=1000nM)} - \theta_{SPR}^{(pDNA=1000nM)} = 6.34 \text{Deg.} \tag{9b}$$

Here, R_{min}^{pDNA} impersonates the minimum reflectance of probe legend, the minimum reflectance of complementary target legend is explained by R_{min}^{ctDNA}, θ_{SPR}^{pDNA} delimitates the SPR angle of pDNAs and at last the SPR angle of sampling complementary target legend is represented by θ_{SPR}^{ctDNA}. Table 4 displays explicit knowledge for when the ctDNAs is inaugurated inside the SPR sensor.

From the obtained outcomes, we can make some decision which is presented in Table 5. On the off chance that the measured values are more prominent than or equivalent to these threshold parameters, at that point we noticed that Complementary DNA hybridization is detected. For explaining detection condition, we obtained a decision and tabulated in Table 5. These values can truly provide a thought regarding fruitful interaction or the failed ones.

The principal condition in Table 5 exposed the aimed state, second and third one needs cautious recheck for achieving wanted shape, the fourth condition affirms the probe is still free and except a target molecule.

Table 4 Measured $\Delta\left[R_{min}^{ctDNA-pDNA}\right]$ and $\Delta\left[\theta_{SPR}^{ctDNA-pDNA}\right]$ values 9 for several concentration of DNA molecules

Concentration (C_a) (nM)	$\Delta R_{min}^{ctDNA-pDNA} = R_{min}^{ctDNA} - R_{min}^{pDNA}$	$\Delta_{spR}^{ctDNA-pDNA} = \theta_{spR}^{ctDNA} - \theta_{spR}^{pDNA}$
1000 (Complementary target)	$\Delta(R_{min}^{ctDNA-pDNA})_{min}$	$\Delta(\theta_{SPR}^{ctDNA-pDNA})_{min}$
1001 (Complementary target)	0.1501	6.34
1010 (Complementary target)	0.1882	6.68
1100 (Complementary target)	0.2520	7.28

Table 5 Four probable conditions for making decision about successful interaction

Conditions for using & Rmin as detecting attributor	Decision
$\Delta R_{min}^{ctDNA-pDNA} \geq (\Delta R_{min}^{ctDNA-pDNA})_{min}$ && $\Delta \theta_{spR}^{ctDNA-pDNA} \geq (\Delta(\theta_{spR}^{ctDNA-pDNA})_{min}$	Complementary DNA hybridization is detected
$\Delta R_{min}^{ctDNA-pDNA} \geq (\Delta R_{min}^{ctDNA-pDNA})_{min}$ && $\Delta \theta_{spR}^{ctDNA-pDNA} \leq \Delta(\theta_{spR}^{ctDNA-pDNA})_{min}$	Re-evaluate
$\Delta R_{min}^{ctDNA-pDNA} \leq (\Delta R_{min}^{ctDNA-pDNA})_{min}$ && $\Delta_{spR}^{ctDNA-pDNA} \geq (\theta_{spR}^{ctDNA-pDNA})_{min}$	Re-evaluate
$\Delta R_{min}^{ctDNA-pDNA} \leq (\Delta R_{min}^{ctDNA-pDNA})_{min}$ && $\Delta_{spR}^{ctDNA-pDNA} \leq \Delta(\theta_{spR}^{ctDNA-pDNA})_{min}$	Single mismatched DNA hybridization is detected

6 Conclusion

In the current work, we have illustrated a refractive index SPR sensor utilizing MoS_2/graphene coatings. The AIM has been utilized for the resolution of reflected optical signal from the sensor consisted prism (SF11 glass), Gold (Au), MoS_2, graphene-based configuration. The effect of adding MoS_2 and graphene layer have been investigated on factors of sensor sensitivity (S), signal to noise ratio (SNR), quality factor (QF), after then these layers are optimized. From the obtained results, we have observed, the angular sensitivity of the optimized structure-based sensor is increased to excellent value of 130 deg-RIU^{-1} with standard angular SNR of 1.37 and QF of 17.02 RIU^{-1}. At last of this paper, an analysis for biomedical application specially for DNA-DNA hybridization has been described. This design capable to recognize the absorption of DNAs onto detecting layer using *ATRM*. The numerical analysis evidence that the dissimilarity of the SPR angle for mismatched DNA strands is very trivial, though that for complementary DNA strands is momentous, which is vital for accurate detection of DNA hybridization.

References

Akimov, Y.A., Koh, W.S.: Resonant and nonresonant plasmonic nanoparticle enhancement for thin-film silicon solar cells. Nanotechnology **21**(23), 235201 (2010)

Avazov, N., Islam, S.R., Park, D., Kwak, K.S.: Statistical characterization of a 3-D propagation model for V2V channels in rectangular tunnels. IEEE Antennas Wirel. Propag. Lett. **16**, 2392–2395 (2017)

Ball, V., Ramsden, J.J.: Buffer dependence of refractive index increments of protein solutions. Biopolymers Original Research on Biomolecules **46**, 489–492 (1998)

Bashiri, J., Rezaei, B., Barvestani, J., Zapata-Rodríguez, C.J.: Bloch surface waves engineering in one-dimensional photonic crystals with a chiral cap layer. JOSA B **36**(8), 2106–2113 (2019)

Diéguez, L., Darwish, N., Mir, M., Martínez, E., Moreno, M., Samitier, J.: Effect of the refractive index of buffer solutions in evanescent optical biosensors. Sens. Lett. **7**(5), 851–855 (2009)

Ebrahimi, S., Sabbaghi-Nadooshan, R., Tavakoli, M.B.: DNA implementation for optical waveguide as a switchable transmission line and memristor. Opt. Quant. Electron. **50**(4), 196 (2018)

Farajollahi, S., AbdollahRamezani, S., Arik, K., Rejae, B., Khavasi, A.: Circuit model for plasmons on graphene with one-dimensional conductivity profile. IEEE Photonics Technol. Lett. **28**(3), 355–358 (2015)

Filion-Côté, S., Roche, P.J., Foudeh, A.M., Tabrizian, M., Kirk, A.G.: Design and analysis of a spectro-angular surface plasmon resonance biosensor operating in the visible spectrum. Rev. Sci. Instrum. **85**(9), 093107 (2014)

Goyal, A.K. and Saini, J., 2020. Performance analysis of Bloch surface wave-based sensor using transition metal dichalcogenides. *Applied Nanoscience*, pp.1–7.

Goyal, A.K. and Pal, S., 2020. Design analysis of Bloch surface wave based sensor for haemoglobin concentration measurement. *APPLIED NANOSCIENCE*..

Heydari, S., Bazgir, M., Zarrabi, F.B., Gandji, N.P., Rastan, I.: Novel optical polarizer design based on metasurface nano aperture for biological sensing in mid-infrared regime. Opt. Quant. Electron. **49**(2), 83 (2017)

Hossain, M.B., Akib, T.B.A., Abdulrazak, L.F., Rana, M.M.: Numerical modeling of graphene-coated fiber optic surface plasmon resonance biosensor for BRCA1 and BRCA2 genetic breast cancer detection. Opt. Eng. **58**(3), 037104 (2019)

Hossain, M.B., Hassan, M., Abdulrazak, L.F., Rana, M.M., Islam, M.M., Rahman, M.S.: Graphene-MoS$_2$-Au-TiO2-SiO2 hybrid SPR biosensor for formalin detection: Numerical analysis and development. Adv. Mater. Lett. **10**(9), 656–662 (2019)

Hossain, M.B., Hossain, M.S., Islam, S.R., Sakib, M.N., Islam, K.Z., Hossain, M.A., Hossain, M.S., Hosen, A.S., Cho, G.H.: Numerical development of high performance quasi D-shape PCF-SPR biosensor: An external sensing approach employing gold. Results in Phys. **18**, 103281 (2020)

Hossain, M., Islam, S.R., Ali, F., Kwak, K.S., Hasan, R.: An internet of things-based health prescription assistant and its security system design. Future Gener CompuT Syst **82**, 422–439 (2018)

Hossain, M.B., Islam, S.R., Hossain, K.T., Abdulrazak, L.F., Sakib, M.N., Amiri, I.S.: High sensitivity hollow core circular shaped PCF surface plasmonic biosensor employing silver coat: A numerical design and analysis with external sensing approach. Results in Phys. **16**, 102909 (2020)

Hossain, M.B., Muktadhir, S., Rana, M.M.: Multi-structural optical devices modeling using graphene tri-layer sheets. Optik **127**(15), 5841–5851 (2016)

Hossain, M.B., Rana, M.M.: Graphene coated high sensitive surface plasmon resonance biosensor for sensing DNA hybridization. Sens. Lett. **13**, 1–8 (2015)

Hossain, M.B., Rana, M.: DNA hybridization detection based on resonance frequency readout in graphene on Au SPR biosensor. J. Sens. **2016**(1), 7 (2016)

Hossain, M.B., Rana, M.M., Abdulrazak, L.F., Mitra, S., Rahman, M.: Graphene-MoS$_2$ with TiO2SiO2 layers based surface plasmon resonance biosensor: Numerical development for formalin detection. Biochem. and Biophys. Rep. **18**, 100639 (2019)

Hossain, M.B., Muktadhir, M.S. and Rana, M.M., 2015, November. Modeling graphene macroscopic and microscopic conductivity in the sub-cell FDTD method. In 2015 International Conference on Electrical & Electronic Engineering (ICEEE) 53–56. IEEE.

Hossain, M.B. and Rana, M.M., 2015, May. An effective compact-FDTD wideband modeling of graphene conductivity. In 2015 International Conference on Electrical Engineering and Information Communication Technology (ICEEICT) 1–3

Islam, S.H., Badrudduza, A.S.M., Islam, S.R., Shahid, F.I., Ansari, I.S., Kundu, M.K., Ghosh, S.K., Hossain, M.B., Hosen, A.S., Cho, G.H.: On secrecy performance of mixed generalized gamma and málaga RF-FSO variable gain relaying channel. IEEE Access **8**, 104127–104138 (2020)

Isti, M.I.A., Talukder, H., Islam, S.R., Nuzhat, S., Hosen, A.S., Cho, G.H., Biswas, S.K.: Asymmetrical D-channel photonic crystal fiber-based plasmonic sensor using the wavelength interrogation and lower birefringence peak method. Results in Phys. **19**, 103372 (2020)

JacobKhurgin, B., Alexandra, Boltasseva: Reflecting upon the losses in plasmonics and metamaterials. MRS Bull. **37**(8), 768–779 (2012)

Kim, M., Park, K., Jeong, E.J., Shin, Y.B., Chung, B.H.: Surface plasmon resonance imaging analysis of protein–protein interactions using on-chip-expressed capture protein. Anal. Biochem. **351**(2), 298–304 (2006)

Kretschmann, E., Raether, H.: Radiative decay of non-radiative surface plasmons excited by light. Z. Naturforsch. a **23**(12), 2135–2136 (1968)

Lee, S.H., Ahn, J.Y., Lee, K.A., Um, H.J., Sekhon, S.S., Park, T.S., Min, J., Kim, Y.H.: Analytical bioconjugates, aptamers, enable specific quantitative detection of Listeria monocytogenes. Biosens. Bioelectron. **68**, 272–280 (2015)

Liedberg, Bo., Nylander, C., Lunström, I.: Surface plasmon resonance for gas detection and biosensing. Sens. and Actuators **4**, 299–304 (1983)

Lin, Z., Jiang, L., Wu, L., Guo, J., Dai, X., Xiang, Y., Fan, D.: Tuning and sensitivity enhancement of surface plasmon resonance biosensor with graphene covered Au-MoS 2-Au films. IEEE Photonics J. **8**(6), 1–8 (2016)

Luo, Y., Chen, C., Xia, K., Peng, S., Guan, H., Tang, J., Lu, H., Yu, J., Zhang, J., Xiao, Y., Chen, Z.: Tungsten disulfide (WS 2) based all-fiber-optic humidity sensor. Opt. Express **24**(8), 8956–8966 (2016)

Madeira, A., Vikeved, E., Nilsson, A., Sjögren, B., Andrén, P.E., Svenningsson, P.: Identification of protein-protein interactions by surface plasmon resonance followed by mass spectrometry. Curr. Protoc. in Protein Sci. **65**(1), 19–21 (2011)

Maurya, J.B., Prajapati, Y.K., Singh, V., Saini, J.P.: Sensitivity enhancement of surface plasmon resonance sensor based on graphene–MoS 2 hybrid structure with TiO 2–SiO 2 composite layer. Appl. Phys. A **121**(2), 525–533 (2015a)

Maurya, J.B., Prajapati, Y.K., Singh, V., Saini, J.P., Tripathi, R.: Performance of graphene–MoS 2 based surface plasmon resonance sensor using silicon layer. Opt. Quant. Electron. **47**(11), 3599–3611 (2015b)

Mollah, M.A., Yousufali, M., Faysal, M.R.B.A., Hasan, M.R., Hossain, M.B., Amiri, I.S.: Highly sensitive photonic crystal fiber salinity sensor based on sagnac interferometer. Results in Phys. **16**, 103022 (2020)

Nico, J. and Fischer, M.J., 2010. Surface plasmon resonance: a general introduction. In Surface Plasmon Resonance (pp. 1–14). Humana Press.

O'Brien, M., Lee, K., Morrish, R., Berner, N.C., McEvoy, N., Wolden, C.A., Duesberg, G.S.: Plasma assisted synthesis of WS2 for gas sensing applications. Chem. Phys. Lett. **615**, 6–10 (2014)

Pockrand, I.: Surface plasma oscillations at silver surfaces with thin transparent and absorbing coatings. Surf. Sci. **72**(3), 577–588 (1978)

Pockrand, I., Swalen, J.D., Gordon Ii, J.G., Philpott, M.R.: Surface plasmon spectroscopy of organic monolayer assemblies. Surf. Sci. **74**(1), 237–244 (1978)

Pumera, M.: Graphene in biosensing. Mater. today **14**(7–8), 308–315 (2011)

Rahman, M.S., Anower, M.S., Rahman, M.K., Hasan, M.R., Hossain, M.B., Haque, M.I.: Modeling of a highly sensitive MoS2-Graphene hybrid based fiber optic SPR biosensor for sensing DNA hybridization. Optik **140**, 989–997 (2017)

Rahman, M.S., Hasan, M.S.M.R., Hossain, M.B., Haque, M.I.: Design and numerical analysis of highly sensitive Au-MoS$_2$-graphene based hybrid surface plasmon resonance biosensor. Optics Commun. **396**, 36–43 (2017)

Rahman, M.S., Hasan, M.R., Rikta, K.A., Anower, M.S.: A novel graphene coated surface plasmon resonance biosensor with tungsten disulfide (WS2) for sensing DNA hybridization. Opt. Mater. **75**, 567–573 (2018)

Rahman, M.S., Hossain, M.B. and Rana, M.M., 2016 Sensitivity enhancement of porous silicon based SPR sensor using graphene-M 0 S 2 hybrid structure. In 2016 2nd International Conference on Electrical, Computer & Telecommunication Engineering (ICECTE) 1–4 IEEE

Rana, M., Hossain, M.B., Islam, R. and Guo, Y.G., 2015, November. Surface plasmon polariton propagation modeling for graphene parallel pair sheets using FDTD. In 2015 IEEE International Conference on Applied Superconductivity and Electromagnetic Devices (ASEMD) 179–180. IEEE.

Saha, S.K., Islam, S.M., Abdullah-AL-Wadud, M., Islam, S., Ali, F., Park, K.S.: Multiomics analysis reveals that GLS and GLS2 differentially modulate the clinical outcomes of cancer. J. Clin. Med. **8**(3), 355 (2019)

Saha, S.K., Islam, S.R., Kwak, K.S., Rahman, M.S., Cho, S.G.: PROM1 and PROM2 expression differentially modulates clinical prognosis of cancer: a multiomics analysis. Cancer Gene. Ther. **27**(3), 147–167 (2020)

Saha, S.K., Saikot, F.K., Rahman, M.S., Jamal, M.A.H.M., Rahman, S.K., Islam, S.R., Kim, K.H.: Programmable molecular scissors: Applications of a new tool for genome editing in biotech. Mol. Ther.Nucleic Acids **14**, 212–238 (2019)

Sakib, M.N., Islam, S.R., Mahendiran, T.V., Abdulrazak, L.F., Islam, M.S., Mehedi, I.M., Kamrunnahar, Q.M., Momtaj, M., Hassan, M.W., Amiri, I.S., Hossain, M.B.: Numerical study of circularly slotted highly sensitive plasmonic biosensor: A novel approach. Results in Phys. **18**, 103130 (2020)

Sarker, N.A., Badrudduza, A.S.M., Islam, S.R., Islam, S.H., Ansari, I.S., Kundu, M.K., Samad, M.F., Hossain, M.B., Yu, H.: Secrecy performance analysis of mixed hyper-gamma and gamma-gamma cooperative relaying system. IEEE Access **8**, 131273–131285 (2020)

Shahzad, M.K., Islam, S.M., Kwak, K.S., Nkenyereye, L.: AEF: Adaptive en-route filtering to extend network lifetime in wireless sensor networks. Sensors **19**(18), 4036 (2019)

Shushama, K.N., Rana, M.M., Inum, R., Hossain, M.B.: Graphene coated fiber optic surface plasmon resonance biosensor for the DNA hybridization detection: Simulation analysis. Optics Commun. **383**, 186–190 (2017a)

Shushama, K.N., Rana, M.M., Inum, R., Hossain, M.B.: Sensitivity enhancement of graphene coated surface plasmon resonance biosensor. Opt. Quant. Electron. **49**(11), 381 (2017b)

Soheilifar, M.R., Zarrabi, F.B.: Reconfigurable metamaterial absorber as an optical switch based on organic-graphene control. Opt. Quant. Electron. **51**(5), 155 (2019)

Sreekanth, K.V., Zeng, S., Yong, K.T., Yu, T.: Sensitivity enhanced biosensor using graphene-based one-dimensional photonic crystal. SenS. and Actuators B: Chem. **182**, 424–428 (2013)

Verma, A., Prakash, A., Tripathi, R.: Sensitivity enhancement of surface plasmon resonance biosensor using graphene and air gap. Optics Commun. **357**, 106–112 (2015)

Wolfbeis, O.S., Weidgans, B.M.: Fiber optic chemical sensors and biosensors: A view back In optical chemical sensors, pp. 17–44. Springer, Dordrecht (2006)

Yuan, Y.J., Gopinath, S.C., Kumar, P.K.: Regeneration of commercial Biacore chips to analyze biomolecular interactions. Opt. Eng. **50**(3), 034402 (2011)

Authors and Affiliations

Md. Biplob Hossain[1] · **Md. Alamgir Kabir[2]** · **Md. Mizanur Rahman[3]** ·
Sourav Roy[4] · **Lway Faisal Abdulrazak[5,6]** · **Md. Sanwar Hossain[2]** · **Nibir Mondol[7]** ·
Mohammed Hadifur Rahman[8] · **Khondoker Ziaul Islam[2]** · **M Ilius Pathan[3]**

Md. Alamgir Kabir
alamgirkabir319@gmail.com

Md. Mizanur Rahman
mizan.eee07@gmail.com

Sourav Roy
souravroy2k9@gmail.com

Lway Faisal Abdulrazak
lway.faisal@sulicihan.edu.krd

Md. Sanwar Hossain
sanwareee@gmail.com

Nibir Mondol
nibir.mondol05@gmail.com

Mohammed Hadifur Rahman
hadifur@mbstu.ac.bd

Khondoker Ziaul Islam
ziaiut@gmail.com

M Ilius Pathan
pmilius2501@gmail.com

[1]   Department of Electrical and Electronic Engineering, Jashore University of Science and Technology, Jashore 7408, Bangladesh

[2]   Department of Electrical and Electronic Engineering, Bangladesh University of Business and Technology, Dhaka 1216, Bangladesh

[3]   Department of Electrical and Electronic Engineering, Hajee Mohammad Danesh Science and Technology University, Dinajpur 5200, Bangladesh

[4]   Department of Mechatronics Engineering, Khulna University of Engineering &Technology, Khulna 9203, Bangladesh

[5]   Department of Computer Science, Cihan University Sulaimaniya, Sulaimaniya 46001, Iraq

[6]   Electrical Engineering Department, College of Engineering, University of Sulaimani, Sulaimaniya 46001, Iraq

[7] Department of Energy Science and Engineering, Khulna University of Engineering and Technology, Khulna 9203, Bangladesh

[8] Department of Competer Science and Engineering, Maolana Bhashani Science and Technology University (MBSTU), Tangail 1902, Bangladesh